Triaxial-shape dynamics in the low-lying excited 0^+ state: Role of the collective mass

Kouhei Washiyama [1,2,*] and Kenichi Yoshida [3,1,4,†]
[1] *Center for Computational Sciences, University of Tsukuba, Tsukuba, Ibaraki 305-8577, Japan*
[2] *Research Center for Superheavy Elements, Kyushu University, Fukuoka 819-0395, Japan*
[3] *Research Center for Nuclear Physics, Osaka University, Ibaraki, Osaka 567-0047, Japan*
[4] *RIKEN Nishina Center for Accelerator-Based Science, Wako, Saitama 351-0198, Japan*

(Received 24 April 2023; revised 29 June 2023; accepted 11 July 2023; published 24 July 2023)

Background: Nonyrast states in neutron-rich nuclei are being investigated experimentally. These states reveal various aspects and details of the nuclear structure, such as the fluctuation around the axially symmetric shape.
Purpose: The beyond-mean-field effects in neutron-rich nuclei with $N \simeq 28$ are investigated. We focus on the role of collective mass in triaxial-shape dynamics.
Method: We employ the five-dimensional quadrupole collective Hamiltonian method with the potential obtained in a constrained Hartree-Fock-Bogoliubov approach with a Skyrme energy-density functional and the collective-mass functions obtained by the cranking approximation. The method includes triaxial deformations.
Results: We find that ^{42}Mg, ^{40}Si, ^{44}S, and ^{46}S show γ-soft: A flat behavior in the potential energy surface along the triaxial deformation. Their low-lying spectra show a strong nucleus dependence, while those obtained with a collective mass assumed as constant are similar to each other. The energy ratio $E(0_2^+)/E(2_1^+)$ and the $B(E2)$ ratio $B(E2; 0_2^+ \to 2_1^+)/B(E2; 2_1^+ \to 0_1^+)$ show a unique property of the 0_2^+ state, while the energy and $B(E2)$ ratios in neutron-deficient γ-soft nuclei with $N = 78$ do not depend on nucleus so much.
Conclusions: Low-lying spectra are determined by not only the potential energy but also the collective mass. We clarify the important role of the collective mass in low-energy dynamics in the neutron-rich $N \approx 28$ nuclei.

DOI: 10.1103/PhysRevC.108.014323

I. INTRODUCTION

Atomic nuclei exhibit various shapes according to the neutron number, the proton number, and the excitation energy. Since the ingredients are finite and their orbital motion is described by quantum mechanics, it is essential to consider the fluctuation in shape. The five-dimensional quadrupole collective Hamiltonian (5DCH) [1–5] as a function of the quadrupole deformation parameters β and γ has often been employed in describing low-energy states. The parameters in the model are the potential energy and the collective masses.

The shape dynamics is governed by the potential energy at first glance. In nuclei near the magic numbers, the potential energy surface (PES) shows the existence of the local minimum at the spherical configuration. As the system moves away from the magic numbers, it becomes deformed, where one mostly has the local minimum at the prolately deformed configuration. Some nuclei show a soft PES against the triaxial deformation. Consequently, the low-lying 2_2^+ state or the so-called γ vibration shows up.

The vibration in the triaxial deformation is not always harmonic. An ideal situation where the PES against the γ direction is flat is investigated by the Wilets-Jean model [6]. In this model, the mass parameters are assumed to be constant. A characteristic feature of the low-lying states is that the 2_2^+ state degenerates with the 4_1^+ state and is lower than the 0_2^+ state among two-phonon states in a spherical harmonic-oscillator potential and that the 0_2^+ is degenerate with the 3_1^+, 4_2^+, and 6_1^+ states. In addition to the flatness in the γ direction, another ideal situation where the PES against the β direction is flat is investigated in terms of the E(5) critical point symmetry [7–10]. The PES in the β direction is described by an infinite square-well potential. The degeneracy of the 2_2^+ and 4_1^+ is the same as in the Wilets-Jean model, while the 0_2^+ state is not necessarily degenerate with the 3_1^+, 4_2^+, and 6_1^+ states because of the fluctuation in the β direction.

Neutron-rich nuclei around $N = 28$ have attracted interest both experimentally [11–21] and theoretically [22–33]. The authors in Refs. [23,28,32] found that the breaking of $N = 28$ magicity in ^{44}S is due to a flat potential, which brings about a wide configuration mixing in the β-γ deformation space. In a neighboring nucleus ^{43}S, the coexistence of prolately, triaxially, and oblately deformed states was predicted due to the breaking of $N = 28$ magicity in Ref. [26]. In $N = 26$ and 30 isotones, it was found that including the triaxial degree of freedom lowers the energy of the 2_2^+ state [27]. The shape coexistence of prolate and oblate configurations and that of oblate and spherical configurations were predicted in ^{40}Mg and ^{42}Si, respectively [28]. The γ vibration was predicted to appear for the prolate configuration in ^{40}Mg [33]. Those studies have shown that the triaxial deformation plays an important role in low-energy dynamics in $N \approx 28$ nuclei.

*washiyama@nucl.ph.tsukuba.ac.jp
†kyoshida@rcnp.osaka-u.ac.jp

Not only the PES but also the mass parameters may play a role in describing the low-energy dynamics in a collective Hamiltonian approach. The mass parameters, as well as the potential energy, depend on the deformations. The terrain of the PES and the deformation-dependence of mass parameters are sensitively determined by the shell effect. Thus by changing the neutron/proton number involving neutron-rich and neutron-deficient nuclei, one can investigate the role of the mass parameters in low-energy dynamics. Therefore, we study in the present work the low-energy dynamics governed by triaxial deformation in neutron-rich nuclei around $N = 28$, putting a focus on the role of the mass parameters in the collective Hamiltonian.

The paper is organized as follows. In Sec. II, we briefly explain the 5DCH method. In Sec. III, we show the results and discuss the roles of the mass parameters. Section IV summarizes the paper.

II. METHOD

We briefly explain the five-dimensional quadrupole collective Hamiltonian method. For details, we refer to Refs. [1–5].

The collective Hamiltonian reads

$$H = T_{\rm vib} + T_{\rm rot} + V(\beta,\gamma), \tag{1}$$

with the vibrational and rotational kinetic energies,

$$T_{\rm vib} = \frac{1}{2}D_{\beta\beta}(\beta,\gamma)\dot{\beta}^2 + D_{\beta\gamma}(\beta,\gamma)\dot{\beta}\dot{\gamma} + \frac{1}{2}D_{\gamma\gamma}(\beta,\gamma)\dot{\gamma}^2, \tag{2}$$

$$T_{\rm rot} = \frac{1}{2}\sum_{k=1}^{3}\mathcal{J}_k(\beta,\gamma)\omega_k^2. \tag{3}$$

The functions $D_{\beta\beta}(\beta,\gamma)$, $D_{\beta\gamma}(\beta,\gamma)$, and $D_{\gamma\gamma}(\beta,\gamma)$ denote the vibrational masses and $\mathcal{J}_k(\beta,\gamma) = 4\beta^2 D_k(\beta,\gamma)\sin^2(\gamma - 2\pi k/3)$ and ω_k denote the rotational moments of inertia and rotational angular velocities in the body-fixed frame of a nucleus. After quantizing the Hamiltonian, we obtain the collective Schrödinger equation as

$$[\hat{T}_{\rm vib} + \hat{T}_{\rm rot} + V(\beta,\gamma)]\Psi_{\alpha IM}(\beta,\gamma,\Omega) = E_{\alpha I}\Psi_{\alpha IM}(\beta,\gamma,\Omega), \tag{4}$$

where $E_{\alpha I}$ and $\Psi_{\alpha IM}(\beta,\gamma,\Omega)$ are the excitation energies and the collective wave functions with the total angular momentum I, its z component M in the laboratory frame, and α distinguishing the states with the same I and M. The collective wave functions are functions of β, γ, and the three Euler angles Ω and are written as

$$\Psi_{\alpha IM}(\beta,\gamma,\Omega) = \sum_{K=\text{even}}^{I}\Phi_{\alpha IK}(\beta,\gamma)\,\langle\Omega|IMK\rangle \tag{5}$$

with $\langle\Omega|IMK\rangle$ being linear combinations of the Wigner rotational wave functions and K being the z component of I in the body-fixed frame. The vibrational wave functions $\Phi_{\alpha IK}(\beta,\gamma)$ are normalized as

$$\int_0^\infty d\beta \int_0^{\pi/3} d\gamma\,|G(\beta,\gamma)|^{1/2} \times \sum_{K=\text{even}}^{I}\Phi^*_{\alpha IK}(\beta,\gamma)\Phi_{\alpha' IK}(\beta,\gamma) = \delta_{\alpha\alpha'}, \tag{6}$$

where the volume element $|G(\beta,\gamma)|^{1/2}$ is given by

$$|G(\beta,\gamma)|^{1/2} = 2\beta^4\sqrt{W(\beta,\gamma)R(\beta,\gamma)}\sin 3\gamma \tag{7}$$

with $W(\beta,\gamma) = \{D_{\beta\beta}(\beta,\gamma)D_{\gamma\gamma}(\beta,\gamma) - [D_{\beta\gamma}(\beta,\gamma)]^2\}\beta^{-2}$ and $R(\beta,\gamma) = D_1(\beta,\gamma)D_2(\beta,\gamma)D_3(\beta,\gamma)$. Using the collective wave functions (5), the reduced quadrupole transition probability is given by

$$B(E2;\alpha I \to \alpha' I') = (2I+1)^{-1}|\,\langle\alpha I||\hat{\mathcal{M}}(E2)||\alpha' I'\rangle\,|^2, \tag{8}$$

where $\hat{\mathcal{M}}(E2)$ is the electric quadrupole operator.

The collective potential $V(\beta,\gamma)$ is obtained by solving the constrained Hartree-Fock-Bogoliubov (CHFB) equation constructed from a Skyrme energy density functional (EDF). The vibrational masses and the rotational moments of inertia are calculated by the so-called cranking approximation [34–36] with the quasiparticle states obtained by the CHFB equation, hereafter denoted as the cranking mass.

We solve the CHFB equation with the two-basis method [37,38] in the three-dimensional Cartesian mesh of $R = 12.4$ fm with the mesh size of 0.8 fm. The single-particle states at positive energies are cut off so as to become the equivalent quasiparticle energy of $E_{\rm QP} \approx 30$ MeV, which gives a good convergence in both the collective potential and the cranking mass in this paper. We used the SkM* EDF [39] and the pairing EDF proposed in Ref. [40], which depends on the isoscalar and isovector densities. Note that, since we used a different pairing cutoff scheme [41,42] from the one in Ref. [40], we refitted the pairing strength to reproduce the neutron pairing gap of ^{156}Dy. For the collective Hamiltonian in the β-γ plane, we employ a triangular mesh of $\Delta\beta \approx 0.035$ in the region $0 < \beta < 0.6$ and $0^\circ < \gamma < 60^\circ$, consisting of about 200 mesh points.

III. RESULTS AND DISCUSSION

Figure 1 shows the PESs in the β-γ plane for the Mg, Si, and S isotopes with $N = 26$, 28, and 30 calculated by the constrained HFB. In the obtained PESs, one sees the minimum at the prolate configuration in ^{38}Mg and ^{42}S and at the oblate configuration in ^{42,44}Si. The PES of ^{40}Mg has two local minima at the prolate and oblate sides. One can see that ^{42}Mg, ^{40}Si, ^{44}S, and ^{46}S possess a unique property that the potential shows a flat behavior from the spherical point to a certain value of β, and along the γ direction, namely γ soft.

To see clearly a γ-soft behavior of PESs, Fig. 2 shows the potential as a function of γ at a fixed β for the nuclei mentioned above. In this figure, the potential is shifted to become $V(\gamma = 0^\circ) = 0$. For each nucleus, the value of β is chosen as its mean value obtained with the ground-state collective wave function ($\alpha = 1, I = K = 0$),

$$\langle\beta\rangle = \int d\beta d\gamma\,|G(\beta,\gamma)|^{1/2}|\Phi_{100}(\beta,\gamma)|^2\beta, \tag{9}$$

and indicated in the figure. The change in potential along the γ direction is 0.2–0.4 MeV.

In what follows, we investigate the low-lying states unique in γ-soft nuclei. The left panels of Fig. 3 show low-lying spectra of ^{44}S (top) and ^{46}S (middle) obtained with the cranking mass. In the spectra, $I \leqslant 6$ in the 0_1^+ band and $I \leqslant 4$ in the

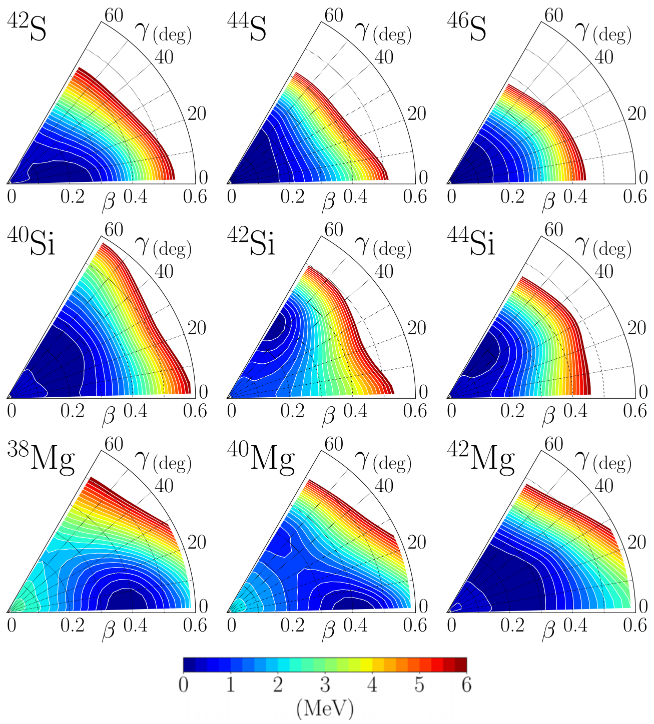

FIG. 1. Potential energy surface in the β-γ plane of Mg, Si, and S isotopes with $N = 26$, 28, and 30 obtained from constrained DFT calculations with the SkM* EDF.

0_2^+ and 2_2^+ bands are plotted and the $B(E2)$ values larger than 1 W.u. are shown. We find that the spectra between ^{44}S and ^{46}S are very different, especially the order of 4_1^+, 2_2^+, and 0_2^+, even though their PESs are very similar to each other as shown in Fig. 1. The energy ratios defined as $R_{0/2} = E(0_2^+)/E(2_1^+)$, $R_{2/2} = E(2_2^+)/E(2_1^+)$, and $R_{4/2} = E(4_1^+)/E(2_1^+)$ are $R_{0/2} =$ 1.65 and 2.45, $R_{2/2} = 1.86$ and 1.89, and $R_{4/2} = 2.34$ and 2.49 for ^{44}S and ^{46}S, respectively. To understand the reason for this difference, we focus on the role of the vibrational and rotational masses on excitation spectra. To this end, we employ the Bohr Hamiltonian with a constant mass [43], where the vibrational and rotational masses obtained by the cranking approximation is replaced by a constant value, neglecting the

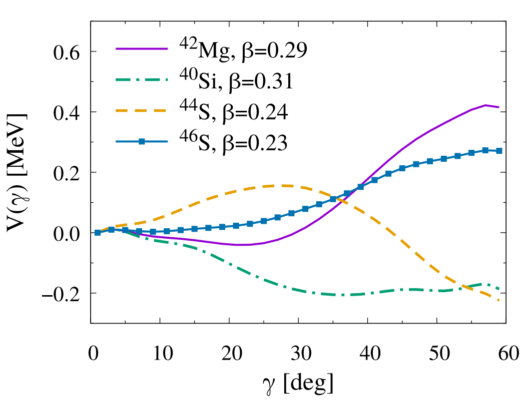

FIG. 2. Potential energy as a function of γ at a fixed β for the selected nuclei. The potential is shifted to $V(\gamma = 0^\circ) = 0$.

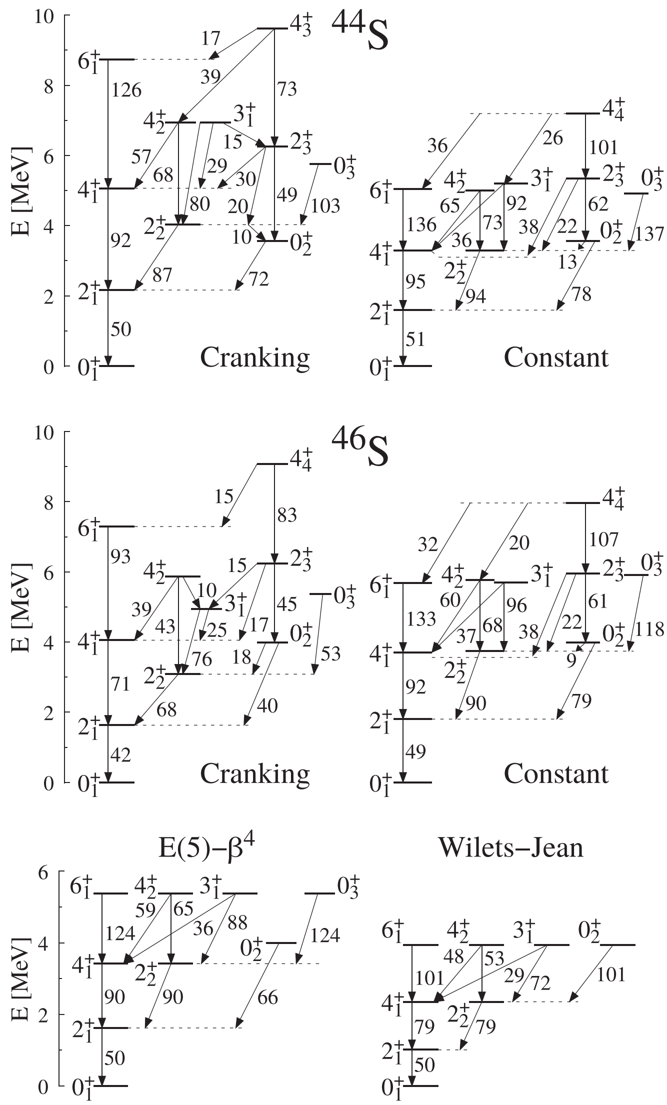

FIG. 3. Low-lying excitation spectra and $B(E2)$ values in units of e^2 fm^4 of ^{44}S (top) and ^{46}S (middle) with the cranking mass (left) and the constant mass (right). Those of the E(5)–β^4 and Wilets-Jean models are shown at the bottom. In the E(5)–β^4 and Wilets-Jean models, the value of D in the constant mass is determined by fitting $E(0_2^+) = 4$ MeV and the $B(E2)$ values are normalized to $B(E2; 2_1^+ \to 0_1^+) = 50\ e^2$ fm^4.

β-γ dependence. Namely [43],

$$D_{\beta\beta} = D_{\gamma\gamma}/\beta^2 = D_1 = D_2 = D_3 \equiv D, \quad D_{\beta\gamma} = 0. \quad (10)$$

The right panels in Fig. 3 show the spectra of ^{44}S and ^{46}S obtained with the constant mass. The value of D is determined to reproduce the 0_2^+ energy obtained with the cranking mass. Clearly, the patterns of the spectra obtained with the constant mass are similar to each other. The energy ratios are $R_{0/2} =$ 2.24 and 2.24, $R_{2/2} = 2.07$ and 2.08, and $R_{4/2} = 2.06$ and 2.06 for ^{44}S and ^{46}S, respectively. Note that how to determine the value of D does not change these energy ratios, though the absolute value of energy changes. If D is determined to give the 2_2^+ energy with the cranking mass, we obtain $R_{0/2} = 2.23$, $R_{2/2} = 2.07$, and $R_{4/2} = 2.06$ for ^{44}S.

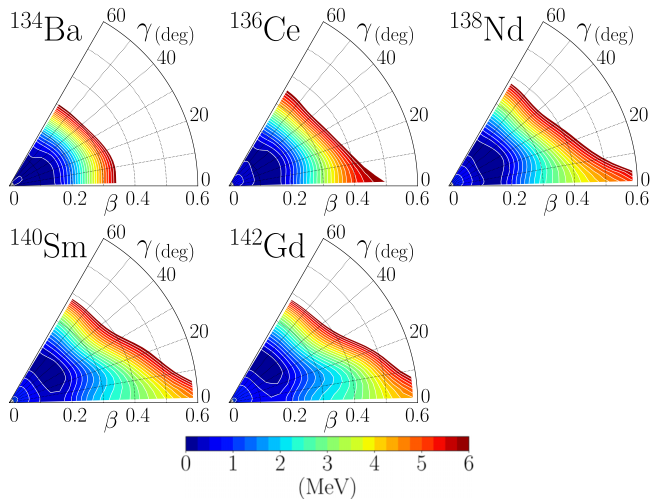

FIG. 4. Same as Fig. 1, but for the neutron-deficient $N = 78$ ^{134}Ba, ^{136}Ce, ^{138}Nd, ^{140}Sm, and ^{142}Gd nuclides.

To see whether the low-lying spectra are sensitive to the collective mass in other mass regions, we study low-energy dynamics of neutron-deficient $N = 78$ nuclei ^{134}Ba, ^{136}Ce, ^{138}Nd, ^{140}Sm, and ^{142}Gd, whose PESs show flat in the β direction and γ soft similarly to those of ^{44}S and ^{46}S. Figures 4 and 5 show how PESs of those nuclei are γ soft. The change in PESs is 0.2–0.6 MeV. As the proton number decreases, the PES becomes flatter.

Figure 6 shows the $R_{4/2}$, $R_{2/2}$, and $R_{0/2}$ values of ^{42}Mg, ^{40}Si, ^{44}S, and ^{46}S and those of the selected $N = 78$ nuclei. The top panel shows the ratios obtained with the cranking mass, while the middle depicts those with the constant mass. In the light nuclei with the cranking mass, $R_{0/2}$ strongly depends on the nucleus, while the variation of $R_{4/2}$ and $R_{2/2}$ is small. The ratios in $N = 78$ nuclei are almost constant, $R_{2/2} \approx 2.0$ and $R_{0/2} \approx R_{4/2} \approx 2.2$–$2.3$ by changing nucleus. Compared with the cranking mass case, the variation of $R_{0/2}$ in the light nuclei becomes significantly small in the constant mass case. In the $N = 78$ nuclei, $R_{4/2}$, $R_{2/2}$, and $R_{0/2}$ values are almost constant around 2.1, 2.1, and 2.5, respectively.

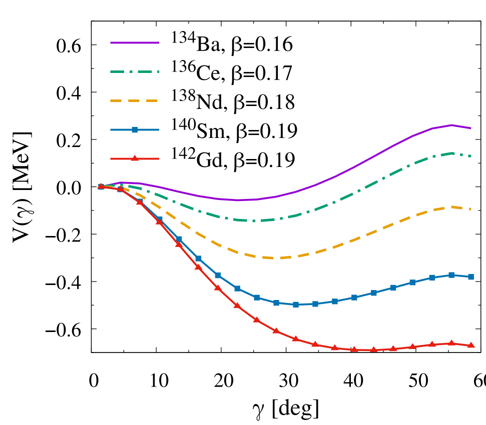

FIG. 5. Same as Fig. 2, but for the $N = 78$ nuclei.

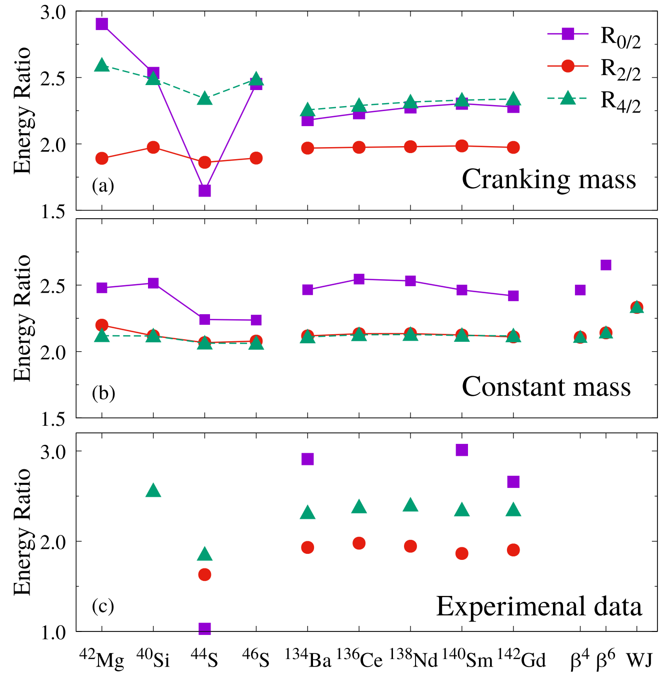

FIG. 6. $R_{0/2}$ (filled square), $R_{2/2}$ (filled circle), and $R_{4/2}$ (filled triangle) for the selected nuclei with the cranking mass (a) and constant mass (b). The ratios obtained with the E(5)–β^4 and E(5)–β^6 models and the Wilets-Jean model (WJ) are included in (b). Note that the $R_{0/2}$ value for the Wilets-Jean model is 3.9. (c) shows the ratios of the available experimental data from [14] for ^{44}S, from [20] for ^{40}Si, and from [44] for the $N = 78$ nuclei.

Properties of the low-energy states in γ-soft nuclei have often been discussed in view of the E(5) critical point symmetry [7–9]. The E(5) symmetry is realized in the Bohr Hamiltonian with an infinite square-well potential in β and a constant in γ. The β^{2n} form of the potential instead of the infinite-well potential is introduced to describe realistic systems [9,10]. In Fig. 6, the energy ratios in the E(5)–β^4 and E(5)–β^6 models are included and denoted as β^4 and β^6, respectively. The energy ratios in the light $N \approx 28$ nuclei and $N = 78$ nuclei with the constant mass are close to those in the E(5)–β^4 and E(5)–β^6 models. The Wilets-Jean model, which describes γ-flat PES, gives higher energy ratios than the ones with the constant mass and with the E(5)–β^4 and E(5)–β^6 models. In the bottom panels of Fig. 3, the low-lying spectra of the E(5)–β^4 and the Wilets-Jean models are shown up to seniority three. These spectra are obtained by $V(\beta, \gamma) = C\beta^4$ with $C = 80$ MeV for E(5)–β^4 and by $V(\beta, \gamma) = C(\beta - 0.3)^2$ with $C = 200$ MeV for the Wilets-Jean model, and with the constant mass D giving $E(0_2^+) = 4$ MeV. The pattern of low-lying spectra in the E(5)–β^4 is close to those of ^{44}S and ^{46}S with the constant mass: The degeneracy of the 2_2^+ and 4_1^+ states and that of the 0_3^+, 3_1^+, 4_2^+, and 6_1^+ states.

The energy ratios obtained from the available experimental data in neutron-rich $N \approx 28$ nuclei are $R_{4/2} = 1.86$, $R_{2/2} = 1.63$ and $R_{0/2} = 1.03$ in ^{44}S [14], and $R_{4/2} = 2.56$ in ^{40}Si [20], as shown in Fig. 6(c). The energy ratio $R_{0/2}$ with the cranking mass shows a strong nucleus dependence in neutron-rich

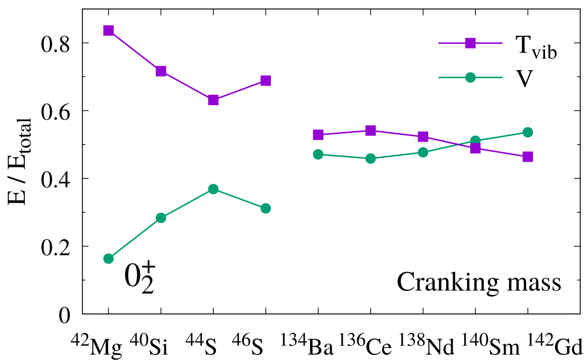

FIG. 7. Decomposition of the 0_2^+ energy to the vibrational kinetic energy $T_{\rm vib}$ and the potential energy V divided by the total energy with the cranking mass for the selected nuclei.

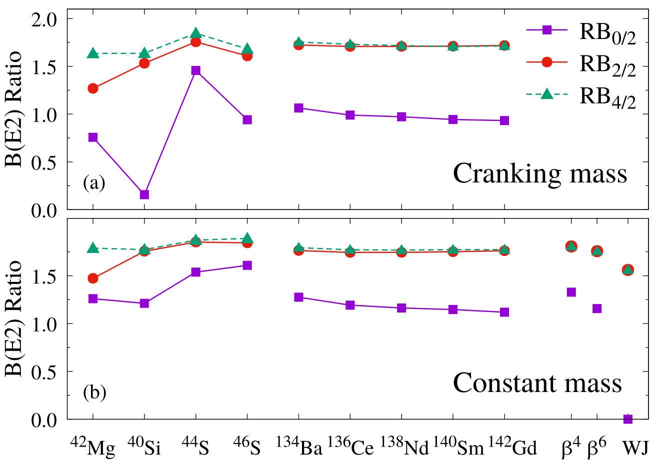

FIG. 8. $B(E2)$ ratio for the selected nuclei with the cranking mass (a) and constant mass (b) together with E(5)–β^4 and E(5)–β^6 models and the Wilets-Jean model (WJ).

$N \approx 28$ nuclei, and one sees a sudden drop in ^{44}S although the measured value is even lower than the calculated one. In the $N = 78$ nuclei, the energy ratios of the available experimental data in Fig. 6(c) are almost constant, though some of the $R_{0/2}$ values are not available. These energy ratios are similar to those with both the cranking and constant mass cases in $N = 78$. More experimental data on the low-lying 0^+ state will give insight into roles of the collective mass.

To further investigate the origin of the different behaviors of $R_{0/2}$ in the $N \approx 28$ and $N = 78$ nuclei, we decompose the energy of the 0_2^+ state to the vibrational kinetic energy and potential energy. These energies are calculated with the vibrational wave function of the 0_2^+ state as

$$E = \int d\beta d\gamma |G(\beta,\gamma)|^{1/2} \Phi^*_{200}(\beta,\gamma) \hat{E} \Phi_{200}(\beta,\gamma), \quad (11)$$

where $\hat{E} = \hat{T}_{\rm vib}$ or $V(\beta,\gamma)$. Figure 7 shows the vibrational kinetic energy $T_{\rm vib}$ and the potential energy V divided by their sum $E_{\rm total} = \langle T_{\rm vib}\rangle + \langle V\rangle$, the absolute value of the 0_2^+ energy, for the $N \approx 28$ and $N = 78$ nuclei. Note that there is no contribution of rotation in the $I = 0$ states. In the $N \approx 28$ nuclei, $T_{\rm vib}$ is larger than V. A large $T_{\rm vib}$ with the deformation-dependent cranking mass enhances the nucleus dependence of the 0_2^+ energy. Furthermore, we found that the ratios of $T_{\rm vib}$, $T_{\rm rot}$, and V to the total energy in the 0_1^+ and 2_1^+ states are almost the same and do not depend on the nucleus so much. Therefore, we observe the strong nucleus-dependent $R_{0/2}$ values. In $N = 78$, the two energies are close to each other and do not much depend on the nucleus. Thus, we have obtained that the $R_{0/2}$ values do not depend on the nucleus even with the deformation-dependent cranking mass.

The similar feature to the energy ratios is indeed obtained in the $B(E2)$ ratios. Figure 8 shows the $B(E2)$ ratios $RB_{0/2} = B(E2; 0_2 \to 2_1)/B(E2; 2_1 \to 0_1)$, $RB_{2/2} = B(E2; 2_2 \to 2_1)/B(E2; 2_1 \to 0_1)$, and $RB_{4/2} = B(E2; 4_1 \to 2_1)/B(E2; 2_1 \to 0_1)$ for the selected nuclei with the cranking mass (top) and the constant mass (bottom). The $RB_{0/2}$ value in the light $N \approx 28$ nuclei with the cranking mass shows a strong dependence on the nucleus. The change in the $RB_{0/2}$ value in the light nuclei with the constant mass is relatively moderate. In the $N = 78$ nuclei, however, all the $B(E2)$ ratios considered do not depend on the nucleus with both the cranking mass and the constant mass. The $B(E2)$ ratios in both the light $N \approx 28$ nuclei and $N = 78$ nuclei with the constant mass are close to those in the E(5)–β^4 and E(5)–β^6 models. These results imply that the 0_2^+ state in the light nuclei is sensitive to the collective mass. We are going to investigate the 0_2^+ state in terms of the collective wave functions below. Furthermore, we conclude that the sensitivity of the collective mass to the low-lying spectra is strong in the light neutron-rich nuclei around $N = 28$ uniquely.

We discuss the structure of the collective wave functions (WFs) of the 0_1^+ and 0_2^+ states. First, we look into the WFs with the constant mass shown in Fig. 9. Here, the WFs are multiplied by $\beta^4\sqrt{W(\beta,\gamma)R(\beta,\gamma)}$, the volume element without $\sin 3\gamma$. The WF of the 0_1^+ state is spread over along the γ direction. This is indeed expected from the γ-soft property in the PESs. The WF of 0_2^+ has a node along the β direction. This is common in ^{44}S and ^{46}S. As expected from the PESs in ^{44}S and ^{46}S, the WFs with the constant mass look similar to those in the E(5)–β^4 model shown in the fifth column in Fig. 9. Next, we discuss the WFs with the cranking mass. The WF of the 0_1^+ state is spread along the γ direction as obtained with the constant mass and peaks at $\gamma \approx 20^\circ$ in ^{44}S and at the oblate side in ^{46}S. The WF of the 0_2^+ state in ^{44}S is more or less similar to that obtained with the constant mass, although the localization around the prolate side is strong. In ^{46}S, the structure of the WF of 0_2^+ is different from that obtained with the constant mass: The WF has two peaks at the prolate and oblate sides. The two-peak structure in the collective WF of the 0_1^+ and 0_2^+ states is a typical feature of shape coexistence, such as in ^{72}Kr [45]. The collective WF of the only 0_2^+ state in ^{46}S looks similar to the collective WFs of the 0_1^+ and 0_2^+ states in ^{72}Kr. Thus, the 0_1^+ and 0_2^+ states in ^{46}S are not interpreted as a usual shape coexistence. This result is rather similar to the one obtained in the Wilets-Jean model shown in the sixth column in Fig. 9.

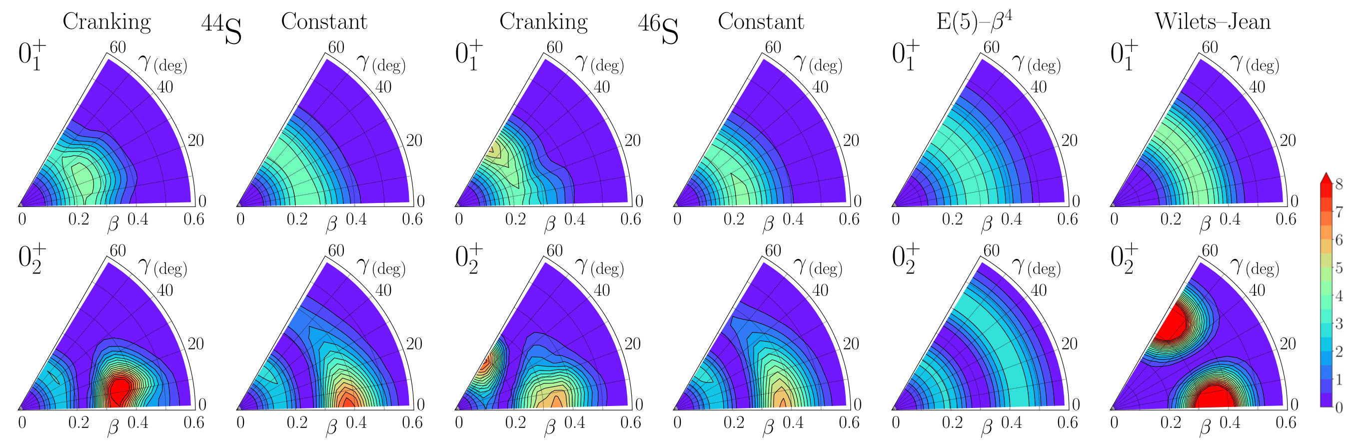

FIG. 9. Vibrational wave functions $|\Psi_{\alpha 00}(\beta,\gamma)|^2$ multiplied by $\beta^4|W(\beta,\gamma)R(\beta,\gamma)|^{1/2}$ of the 0_1^+ (top) and 0_2^+ (bottom) states with the cranking and constant masses for ^{44}S and ^{46}S. The right two columns show those with the E(5)–β^4 and Wilets-Jean models.

IV. SUMMARY

We have investigated the role of the mass parameters in the collective Hamiltonian for the triaxial-shape dynamics in neutron-rich nuclei with $N \simeq 28$. The PESs are obtained by the constrained HFB method with a Skyrme-type EDF. We found that the PES in ^{42}Mg, ^{40}Si, ^{44}S, and ^{46}S possesses a topography similar to each other and is soft against triaxial deformation. The low-lying spectra obtained by assuming the mass parameters as constant are similar. However, the spectra obtained considering the deformation dependence of the mass parameters with the cranking approximation show characteristic features. The second 0^+ state is sensitive to the treatment of the mass parameters. The energy ratio $R_{0/2}$ and the $B(E2)$ ratio $RB_{0/2}$ show a strong nucleus dependence. The dependence of $R_{0/2}$ and $RB_{0/2}$ on the nucleus in neutron-deficient $N = 78$ nuclei, which also exhibit the γ-soft nature, is less pronounced. We clarified the unique role of the collective mass in $N \approx 28$ nuclei.

ACKNOWLEDGMENTS

The authors thank M. Kimura and Y. Suzuki for the valuable discussions. This work was supported by JSPS KAKENHI (Grants No. JP19K03824 and No. JP19K03872) and the JSPS/NRF/NSFC A3 Foresight Program "Nuclear Physics in the 21st Century."

[1] J. Libert, M. Girod, and J.-P. Delaroche, Microscopic descriptions of superdeformed bands with the Gogny force: Configuration mixing calculations in the $A \sim 190$ mass region, Phys. Rev. C **60**, 054301 (1999).

[2] L. Próchniak, P. Quentin, D. Samsoen, and J. Libert, A self-consistent approach to the quadrupole dynamics of medium heavy nuclei, Nucl. Phys. A **730**, 59 (2004).

[3] T. Nikšić, Z. P. Li, D. Vretenar, L. Próchniak, J. Meng, and P. Ring, Beyond the relativistic mean-field approximation. III. Collective Hamiltonian in five dimensions, Phys. Rev. C **79**, 034303 (2009).

[4] J.-P. Delaroche, M. Girod, J. Libert, H. Goutte, S. Hilaire, S. Péru, N. Pillet, and G. F. Bertsch, Structure of even-even nuclei using a mapped collective Hamiltonian and the D1S Gogny interaction, Phys. Rev. C **81**, 014303 (2010).

[5] K. Matsuyanagi, M. Matsuo, T. Nakatsukasa, K. Yoshida, N. Hinohara, and K. Sato, Microscopic derivation of the Bohr-Mottelson collective Hamiltonian and its application to quadrupole shape dynamics, Phys. Scr. **91**, 063014 (2016).

[6] L. Wilets and M. Jean, Surface oscillations in even-even nuclei, Phys. Rev. **102**, 788 (1956).

[7] F. Iachello, Dynamic Symmetries at the Critical Point, Phys. Rev. Lett. **85**, 3580 (2000).

[8] R. F. Casten and N. V. Zamfir, Evidence for a Possible E(5) Symmetry in ^{134}Ba, Phys. Rev. Lett. **85**, 3584 (2000).

[9] R. F. Casten, Shape phase transitions and critical-point phenomena in atomic nuclei, Nat. Phys. **2**, 811 (2006).

[10] D. Bonatsos, D. Lenis, N. Minkov, P. P. Raychev, and P. A. Terziev, Sequence of potentials interpolating between the U(5) and E(5) symmetries, Phys. Rev. C **69**, 044316 (2004).

[11] D. Sohler, Z. Dombrádi, J. Timár, O. Sorlin, F. Azaiez, F. Amorini, M. Belleguic, C. Bourgeois, C. Donzaud, J. Duprat, D. Guillemaud-Mueller, F. Ibrahim, J. A. Scarpaci, M. Stanoiu, M. J. Lopez, M. G. Saint-Laurent, F. Becker, F. Sarazin, C. Stodel, G. Voltolini *et al.*, Shape evolution in heavy sulfur isotopes and erosion of the $N = 28$ shell closure, Phys. Rev. C **66**, 054302 (2002).

[12] B. Longfellow, D. Weisshaar, A. Gade, B. A. Brown, D. Bazin, K. W. Brown, B. Elman, J. Pereira, D. Rhodes, and M. Spieker, Quadrupole collectivity in the neutron-rich sulfur isotopes ^{38,40,42,44}S, Phys. Rev. C **103**, 054309 (2021).

[13] C. Force, S. Grévy, L. Gaudefroy, O. Sorlin, L. Cáceres, F. Rotaru, J. Mrazek, N. L. Achouri, J. C. Angélique, F. Azaiez, B. Bastin, R. Borcea, A. Buta, J. M. Daugas, Z. Dlouhy, Z. Dombrádi, F. De Oliveira, F. Negoita, Y. Penionzhkevich, M. G. Saint-Laurent *et al.*, Prolate-Spherical Shape Coexistence at $N = 28$ in ^{44}S, Phys. Rev. Lett. **105**, 102501 (2010).

[14] D. Santiago-Gonzalez, I. Wiedenhöver, V. Abramkina, M. L. Avila, T. Baugher, D. Bazin, B. A. Brown, P. D. Cottle, A. Gade, T. Glasmacher, K. W. Kemper, S. McDaniel, A. Rojas,

A. Ratkiewicz, R. Meharchand, E. C. Simpson, J. A. Tostevin, A. Volya, and D. Weisshaar, Triple configuration coexistence in ^{44}S, Phys. Rev. C **83**, 061305(R) (2011).

[15] L. Gaudefroy, J. M. Daugas, M. Hass, S. Grévy, C. Stodel, J. C. Thomas, L. Perrot, M. Girod, B. Rossé, J. C. Angélique, D. L. Balabanski, E. Fiori, C. Force, G. Georgiev, D. Kameda, V. Kumar, R. L. Lozeva, I. Matea, V. Méot, P. Morel *et al.*, Shell Erosion and Shape Coexistence in $^{43}_{16}$S$_{27}$, Phys. Rev. Lett. **102**, 092501 (2009).

[16] T. Mijatović, N. Kobayashi, H. Iwasaki, D. Bazin, J. Belarge, P. C. Bender, B. A. Brown, A. Dewald, R. Elder, B. Elman, A. Gade, M. Grinder, T. Haylett, S. Heil, C. Loelius, B. Longfellow, E. Lunderberg, M. Mathy, K. Whitmore, and D. Weisshaar, Lifetime Measurements and Triple Coexisting Band Structure in ^{43}S, Phys. Rev. Lett. **121**, 012501 (2018).

[17] B. Longfellow, D. Weisshaar, A. Gade, B. A. Brown, D. Bazin, K. W. Brown, B. Elman, J. Pereira, D. Rhodes, and M. Spieker, Shape Changes in the $N = 28$ Island of Inversion: Collective Structures Built on Configuration-Coexisting States in ^{43}S, Phys. Rev. Lett. **125**, 232501 (2020).

[18] C. M. Campbell, N. Aoi, D. Bazin, M. D. Bowen, B. A. Brown, J. M. Cook, D.-C. Dinca, A. Gade, T. Glasmacher, M. Horoi, S. Kanno, T. Motobayashi, W. F. Mueller, H. Sakurai, K. Starosta, H. Suzuki, S. Takeuchi, J. R. Terry, K. Yoneda, and H. Zwahlen, Measurement of Excited States in ^{40}Si and Evidence for Weakening of the $N = 28$ Shell Gap, Phys. Rev. Lett. **97**, 112501 (2006).

[19] B. Bastin, S. Grévy, D. Sohler, O. Sorlin, Z. Dombrádi, N. L. Achouri, J. C. Angélique, F. Azaiez, D. Baiborodin, R. Borcea, C. Bourgeois, A. Buta, A. Bürger, R. Chapman, J. C. Dalouzy, Z. Dlouhy, A. Drouard, Z. Elekes, S. Franchoo, S. Iacob *et al.*, Collapse of the $N = 28$ Shell Closure in ^{42}Si, Phys. Rev. Lett. **99**, 022503 (2007).

[20] S. Takeuchi, M. Matsushita, N. Aoi, P. Doornenbal, K. Li, T. Motobayashi, H. Scheit, D. Steppenbeck, H. Wang, H. Baba, D. Bazin, L. Càceres, H. Crawford, P. Fallon, R. Gernhäuser, J. Gibelin, S. Go, S. Grévy, C. Hinke, C. R. Hoffman *et al.*, Well Developed Deformation in ^{42}Si, Phys. Rev. Lett. **109**, 182501 (2012).

[21] H. L. Crawford, P. Fallon, A. O. Macchiavelli, P. Doornenbal, N. Aoi, F. Browne, C. M. Campbell, S. Chen, R. M. Clark, M. L. Cortés, M. Cromaz, E. Ideguchi, M. D. Jones, R. Kanungo, M. MacCormick, S. Momiyama, I. Murray, M. Niikura, S. Paschalis, M. Petri *et al.*, First Spectroscopy of the Near Drip-Line Nucleus ^{40}Mg, Phys. Rev. Lett. **122**, 052501 (2019).

[22] R. Rodríguez-Guzmán, J. L. Egido, and L. M. Robledo, Quadrupole collectivity in $N \approx 28$ nuclei with the angular momentum projected generator coordinate method, Phys. Rev. C **65**, 024304 (2002).

[23] T. R. Rodríguez and J. L. Egido, Configuration mixing description of the nucleus ^{44}S, Phys. Rev. C **84**, 051307(R) (2011).

[24] J. L. Egido, M. Borrajo, and T. R. Rodríguez, Collective and Single-Particle Motion in Beyond Mean Field Approaches, Phys. Rev. Lett. **116**, 052502 (2016).

[25] J. M. Yao, H. Mei, H. Chen, J. Meng, P. Ring, and D. Vretenar, Configuration mixing of angular-momentum-projected triaxial relativistic mean-field wave functions. II. Microscopic analysis of low-lying states in magnesium isotopes, Phys. Rev. C **83**, 014308 (2011).

[26] M. Kimura, Y. Taniguchi, Y. Kanada-En'yo, H. Horiuchi, and K. Ikeda, Prolate, oblate, and triaxial shape coexistence, and the lost magicity of $N = 28$ in ^{43}S, Phys. Rev. C **87**, 011301(R) (2013).

[27] Y. Suzuki and M. Kimura, Triaxial deformation and the disappearance of the $N = 28$ shell gap, Phys. Rev. C **104**, 024327 (2021).

[28] Y. Suzuki, W. Horiuchi, and M. Kimura, Erosion of $N = 28$ shell closure: Shape coexistence and monopole transition, Prog. Theor. Exp. Phys. **2022**, 063D02 (2022).

[29] Y. Utsuno, T. Otsuka, B. A. Brown, M. Honma, T. Mizusaki, and N. Shimizu, Shape transitions in exotic Si and S isotopes and tensor-force-driven Jahn-Teller effect, Phys. Rev. C **86**, 051301(R) (2012).

[30] Y. Utsuno, N. Shimizu, T. Otsuka, T. Yoshida, and Y. Tsunoda, Nature of Isomerism in Exotic Sulfur Isotopes, Phys. Rev. Lett. **114**, 032501 (2015).

[31] K. Yoshida, Cranked Skyrme-Hartree-Fock-Bogoliubov approach for a mean-field description of nuclear rotations near the drip line, Phys. Rev. C **105**, 024313 (2022).

[32] Z. P. Li, J. M. Yao, D. Vretenar, T. Nikšić, H. Chen, and J. Meng, Energy density functional analysis of shape evolution in $N = 28$ isotones, Phys. Rev. C **84**, 054304 (2011).

[33] K. Yoshida, Skyrme-QRPA calculations for low-lying excitation modes in deformed neutron-rich nuclei, Eur. Phys. J. A **42**, 583 (2009).

[34] D. R. Inglis, Nuclear moments of inertia due to nucleon motion in a rotating well, Phys. Rev. **103**, 1786 (1956).

[35] S. T. Beliaev, Concerning the calculation of the nuclear moment of inertia, Nucl. Phys. **24**, 322 (1961).

[36] M. Girod and B. Grammaticos, The zero-point energy correction and its effect on nuclear dynamics, Nucl. Phys. A **330**, 40 (1979).

[37] B. Gall, P. Bonche, J. Dobaczewski, H. Flocard, and P.-H. Heenen, Superdeformed rotational bands in the mercury region. A cranked Skyrme-Hartree-Fock-Bogoliubov study, Z. Phys. A **348**, 183 (1994).

[38] J. Terasaki, P.-H. Heenen, P. Bonche, J. Dobaczewski, and H. Flocard, Superdeformed rotational bands with density dependent pairing interactions, Nucl. Phys. A **593**, 1 (1995).

[39] J. Bartel, P. Quentin, M. Brack, C. Guet, and H.-B. Håkansson, Towards a better parametrisation of Skyrme-like effective forces: A critical study of the SkM force, Nucl. Phys. A **386**, 79 (1982).

[40] M. Yamagami, Y. R. Shimizu, and T. Nakatsukasa, Optimal pair density functional for the description of nuclei with large neutron excess, Phys. Rev. C **80**, 064301 (2009).

[41] P. Bonche, H. Flocard, P.-H. Heenen, S. J. Krieger, and M. S. Weiss, Self-consistent study of triaxial deformations: Application to the isotopes of Kr, Sr, Zr and Mo, Nucl. Phys. A **443**, 39 (1985).

[42] P. Bonche, H. Flocard, and P.-H. Heenen, Solution of the Skyrme HF+BCS equation on a 3D mesh, Comput. Phys. Commun. **171**, 49 (2005).

[43] A. Bohr, Mat. Fys. Medd. Dan. Vid. Selsk. **26**, 14 (1952).

[44] National Nuclear Data Center, Brookhaven National Laboratory, https://www.nndc.bnl.gov/nudat3/.

[45] K. Sato and N. Hinohara, Shape mixing dynamics in the low-lying states of proton-rich Kr isotopes, Nucl. Phys. A **849**, 53 (2011).